Connecting scaling with short-range correlations

D. Berardo,[1] M. B. Barbaro,[2] R. Cenni,[3] T. W. Donnelly,[4] and A. Molinari[2]

[1]*Dipartimento di Fisica Teorica, Università di Torino, Via Pirtro Giuria 1, IT-10125 Torino, Italy*
[2]*Dipartimento di Fisica Teorica, Università di Torino and INFN, Sezione di Torino, Via Pietro Giuria 1, IT-10125 Torino, Italy*
[3]*INFN, Sezione di Genova, Via Dodecaneso 33, IT-16146 Genova, Italy*
[4]*Center for Theoretical Physics, Laboratory for Nuclear Science and Department of Physics, Massachusetts Institute of Technology, Cambridge, Massachusetts 02139, USA*

We reexamine several issues related to the physics of scaling in electron scattering from nuclei. A basic model is presented in which an assumed form for the momentum distribution having both long- and short-range contributions is incorporated in the single-particle Green's function. From this one can obtain saturation of nuclear matter for an NN interaction with medium-range attraction and short-range repulsion and obtain the density-density polarization propagator and, hence, the electromagnetic response and scaling function. For the latter, the shape of the scaling function and how it approaches scaling as a function of momentum transfer are both explored.

I. INTRODUCTION

Scaling phenomena as realized in electroweak interactions with nuclei at intermediate-to-high energies have several facets, including scaling of the first kind [1] (independence of the momentum transfer q) and second kind [2,3] (independence of nuclear species, for instance, as characterized by the Fermi momentum k_F). In addition, universality for different reaction channels (longitudinal, transverse, etc.) has been called scaling of the zeroth kind [3,4], while universality in the isoscalar and isovector channels has been called scaling of the third kind [5]. All four types of scaling are reasonably well respected by data at sufficiently high energies, namely, away from threshold and for momentum transfers typically twice the Fermi momentum or larger, although there are observed to be scaling violations and their origins provide interesting insights into the dynamics of the scattering processes. For example, the transverse EM response is known to involve both the familiar one-body currents and two-body meson-exchange currents (MECs) which do not scale in the same way [6–10].

In the present study we focus on one particular aspect of scaling, namely, scaling of the first kind. Our motivation is to explore the interconnections between the strong interaction dynamics of a representative NN potential that is chosen to provide the correct binding energy and saturation density of nuclear matter on the one hand and a corresponding Green's function that is made to be consistent with those properties of nuclear matter on the other. Having such a Green's function one can immediately obtain the density-density polarization propagator and hence the longitudinal response R_L and scaling function F_L. For brevity these are called simply R and F in the rest of this work. In contrast to the usual approach, in the present study we "work backward," assuming a form for the momentum distribution $n(k)$ and, given this, obtaining the corresponding energy per particle as a consequence. In particular, the chosen momentum distribution is taken to have both long-range contributions (those below and slightly above the Fermi surface) and short-range contributions which give

rise to a tail that extends to high momentum, but which are, in fact, operative at any momentum.

To be able to carry out this study with much of the development still analytic we restrict our attention to the nonrelativistic situation and assume a translationally invariant (infinite, homogeneous) many-body system of point nucleons. Our goal is not to provide a detailed numerical study of scaling phenomena for comparison with experiment, as this is better done with relativistic modeling, but is to provide insight into how the short-range part of the momentum distribution which is important for obtaining saturation of nuclear matter also has a role to play in the corresponding scaling phenomena. We shall thus explore several properties of scaling and scaling violations that are observed experimentally, namely, how scaling is approached for large momentum transfers q (in the scaling region it is approached from above, something most models fail to explain) and whether or not the present model is capable of explaining the observed asymmetry found in the scaling function.

In passing, let us draw some comparisons with deep inelastic scattering (DIS) of leptons on the proton which has been understood on the basis of the Bjorken scaling law and the parton model. There also one observes scaling violations which in the high-energy situation are coped with using the so-called evolution equations. Two basic assumptions lie at the foundations of Bjorken scaling (see, for example, Ref. [11]): (1) The highly virtual photon interacts with the proton through pointlike constituents (the partons) and (2) the partons cannot change their momenta during the extremely short time interval available for the DIS process and the parton-parton interactions are very weak, a situation referred to as asymptotic freedom. When taken into account the latter leads to scaling violations. In contrast, the situation of interest in the present work on electron scattering from strongly interacting nucleons in nuclei is apparently quite different. The model we use does not display the equivalent of asymptotic freedom and yet scaling is quite well obeyed, despite the strength of the

partonic (nucleonic here) interactions. Of course, our model is not able to account for all types of scaling violations, namely, those that stem from partonic substructures (gluons in QCD versus mesons in nuclei via MECs; the latter have been the subject in other studies, for instance, Refs. [7,8]). In other words, our nucleons (partons) are viewed as pointlike. The very strong correlations between the nucleons induced by the short-range repulsion appear, at least in our model, to lend themselves to a description in terms of a mean field framework, in which the nucleons do not interact, apart from Pauli correlations. In other words, the effect of the hard core is embedded in the modification of the nucleon momentum distribution with respect to that of the Fermi gas, still keeping an independent-particle model for the system. Thus, to the extent that our single-particle propagator of mean-field type provides a realistic description of nuclei at large momenta, scaling should occur, as we have found.

This paper, which is closely connected to the research developed in Ref. [12], outlines the model in Sec. II. Section III addresses the problems of linking the model to conventional perturbation theory and focuses on the Coulomb sum rule (CSR), a quantity crucially dependent upon the pair correlation function (pcf) or, equivalently, upon the momentum distribution $n(k)$ of the nucleons in the nucleus. Indeed the CSR represents one of the best testing grounds for the pcf and $n(k)$. In Sec. IV a model for the fermion propagator, the key element in constructing the response of our system to an external probe and hence the scaling function, is set up. All the issues connected with scaling and the results we have obtained with our approach are collected in Sec. V and then, finally, in Sec. VI we summarize our main conclusions from this study.

II. THE MODEL

The basic formula we start with reads [13] (we use $\hbar = c = 1$)

$$
\frac{E}{A} = \frac{4V}{A} \int \frac{d\vec{k}}{(2\pi)^3} \frac{k^2}{2m} n(k)
$$
$$
+ \frac{1}{2A} \int d\vec{r}_1 d\vec{r}_2 v(\vec{r}_1 - \vec{r}_2) C(\vec{r}_1 - \vec{r}_2), \quad (1)
$$

where the factor of 4 accounts for the spin-isospin degeneracy (a summation over these variables is of course understood in the second term as well) and A is the particle number. Equation (1) yields the ground-state energy of the system (actually the energy per particle). We apply it to an infinite, homogeneous, nonrelativistic ensemble of nucleons, viewed as enclosed in

a large volume V to be let to go to infinity at the end of the calculation. We assume that a two-body force acts between the nucleons and that this is described by the potential $v(r)$, where $r = |\vec{r}_1 - \vec{r}_2|$. In Eq. (1) $C(\vec{r}_1 - \vec{r}_2)$ is the pcf simply related by a Fourier transform to the $n(k)$ in our spatially homogeneous system.

Now, rather than attempting to compute $n(k)$ starting from the potential $v(r)$ adopting one of the various many-body techniques available for the purpose (for example, a perturbative one), we *assume* the momentum distribution to be parametrized as

$$
n(k) = \theta(k_F - k)\left(1 - \alpha \frac{k^2}{k_F^2}\right) + \theta(k - k_F)\beta_1 e^{-\beta_2\left(\frac{k}{k_F} - 1\right)},
$$
$$
(2)
$$

accounting both for the existence of a high-momentum tail in $n(k)$, as suggested by the presently available experimental information, as well as standard theory (see, for example, a recent treatment of the momentum distribution and spectral function in Ref. [14]), and for the Luttinger theorem, which guarantees the existence of a Fermi surface for a "normal" interacting Fermi system. Of course, $n(k)$ [Eq. (2)] should fulfill the constraint

$$
\frac{A}{V} = 4 \int \frac{d\vec{k}}{(2\pi)^3} n(k) = \frac{2}{\pi^2}\left\{\int_0^{k_F} k^2 dk\left(1 - \alpha\frac{k^2}{k_F^2}\right)\right.
$$
$$
\left. + \beta_1 \int_{k_F}^{\infty} k^2 dk e^{-\beta_2\left(\frac{k}{k_F} - 1\right)}\right\}
$$
$$
= \frac{2k_F^3}{3\pi^2}\left[1 - \alpha\frac{3}{5} + 3\frac{\beta_1}{\beta_2^3}\left(\beta_2^2 + 2\beta_2 + 2\right)\right]
$$
$$
= \frac{2k_F^3}{3\pi^2} h(\alpha, \beta_1, \beta_2) = n_0, \quad (3)
$$

n_0 being the system's constant density.

It should be stressed that Eq. (2) is just meant to be a simple parametrization of what has been done in the literature with more sophisticated modeling (see, for instance, Refs. [15–18]) and is supposed to capture both short- and long-range correlations in a simple form that allows for analytic calculations. Moreover, here we are dealing with an infinite system; when finite-nucleus Hartree-Fock (HF) calculations are done with typical (soft) interactions $n(k)$ does have a softened Fermi surface. However, without strong repulsive cores as in Brueckner-HF theory [15,17], one does not see a tail extending to very large momenta, but has a very rapid drop-off with k once one goes only slightly beyond k_F.

From Eq. (2) the pcf is obtained according to the definition

$$
C(\vec{r}_1 - \vec{r}_2) = \sum_{\gamma,\delta} \langle\Psi_0|\hat{\Psi}_\gamma^\dagger(\vec{r}_1)\hat{\Psi}_\delta^\dagger(\vec{r}_2)\hat{\Psi}_\delta(\vec{r}_2)\hat{\Psi}_\gamma(\vec{r}_1)|\Psi_0\rangle
$$

$$
= \left(\frac{A}{V}\right)^2 - 4\left[h(\alpha, \beta_1, \beta_2)\int \frac{d\vec{k}}{(2\pi)^3} e^{-i\vec{k}\cdot\vec{r}} n(k)\right]^2
$$

$$
= n_0^2\left\{1 - \frac{1}{4}g^2(r)\right\} \quad (4)
$$

and one gets

$$C(r) = n_0^2 \left\{ 1 - \frac{1}{4} \left\{ \frac{3}{k_F r} \left[j_1(k_F r) - \frac{\alpha}{(k_F r)^4} (3((k_F r)^2 - 2)\sin(k_F r) - k_F r((k_F r)^2 - 6)\cos(k_F r)) + \beta_1 \left(\frac{k_F r}{(k_F r)^2 + \beta_2^2} \right)^2 \right. \right. \right.$$

$$\left. \left. \left. \times \left(\sin(k_F r) \left(\beta_2 + \frac{\beta_2^2 + \beta_2^3}{(k_F r)^2} - 1 \right) + \cos(k_F r) \left(k_F r + \frac{2\beta_2 + \beta_2^2}{k_F r} \right) \right) \right] \right\}^2 \right\}. \tag{5}$$

In Eq. (4) $|\Psi_0\rangle$ is the system's ground state and $\hat{\Psi}_\gamma(\vec{r}_1)$ and $\hat{\Psi}_\delta(\vec{r}_2)$ are the fermion fields. Furthermore, the above formula holds for infinite nuclear matter. If we need the pcf only for protons, as in the case of the CSR, then the factor $\frac{1}{4}$ should clearly be replaced with a factor $\frac{1}{2}$ in front of the second term on the right-hand side of Eq. (5) and one should set $n_0 = Z/V$, Z being the number of protons. As seen in the above equations, the pcf naturally splits into a direct and an exchange contribution [the first and the second terms on the right-hand side of Eq. (4)].

In passing we note that by setting $\alpha = \beta_1 = 0$ for any $\beta_2 \geqslant 0$ in Eq. (5), we recover in Eq. (2) the θ-function momentum distribution of a noninteracting Fermi system, whereas from Eqs. (3) and (5), but with $\beta_2 > 0$, we get back the well-known density $n_0 = 2k_F^3/3\pi^2$ and pcf of a Fermi gas,

$$C(r) = n_0^2 \left[1 - \frac{1}{4} \left(\frac{3 j_1(k_F r)}{k_F r} \right)^2 \right], \tag{6}$$

which identifies $g(r)$ with $\frac{3 j_1(k_F r)}{k_F r}$.

Now by inserting Eqs. (2) and (5) into Eq. (1) we obtain the binding energy per particle of the nuclear system providing the

potential $v(r)$ is known. For the latter we employ a schematic model which retains only the basic features of the nucleon-nucleon force because, as already emphasized, our aim is not a precise reproduction of the experimental data. Accordingly, we employ a mixture of a Wigner and a Majorana force, namely,

$$v(r) = u(r)[1 - \gamma + \gamma P_x] = \begin{cases} +U_0 \ \gamma = 0 & r \leqslant a, \\ -V_0 \ \gamma = \frac{1}{2} & a \leqslant r \leqslant b, \\ 0 & b \leqslant r, \end{cases} \tag{7}$$

where P_x is the space exchange operator and γ a parameter varying in the range $0 \leqslant \gamma \leqslant 1$. In accord with common wisdom, we choose for γ the values indicated in Eq. (7), where one recognizes the strong short-range repulsion and the moderate intermediate-range attraction characterizing the nucleon-nucleon interaction. Actually, in the present scheme, the instantaneous potential (7) is meant to represent an effective NN interaction in the medium arising from the the ladder diagrams summed up via the Bethe-Goldstone equation, but ignoring all the energy and momentum dependence.

Now all of the elements to compute the behavior of the E/A versus k_F are available. We get

$$\frac{E}{A} = \frac{4}{n_0} \frac{4\pi}{(2\pi)^3} \frac{1}{2m} \int_0^\infty dk\, k^4 n(k) + \frac{n_0}{2} 4\pi \int_0^\infty dr\, r^2 \left[U_0 \theta(a - r) - \frac{3}{8} V_0 \theta(b - r)\theta(r - a) \right]$$

$$- \frac{n_0}{2} \frac{1}{4} 4\pi \int_0^\infty dr\, r^2 \left[U_0 \theta(a - r) + \frac{3}{2} V_0 \theta(b - r)\theta(r - a) \right] g^2(r). \tag{8}$$

The numerical factors appearing in the potential terms stem from summing over the spin-isospin variables of the interacting nucleons; they, of course, enter differently in the direct and exchange contributions to E/A, namely, the second and the third terms on the right-hand side of Eq. (8).

Before actually displaying the behavior of E/A versus k_F we have to face the crucial problem of fixing the values of the seven parameters [four for the potential $v(r)$, three for the momentum distribution $n(k)$] needed to render our approach predictive. To tackle this problem we proceed as follows. We start by choosing "reasonable" values. Next we compute Eq. (8) using these chosen values and repeat the procedure adjusting at each step the parameters until they yield $E/A \sim -16$ MeV and, for the compression modulus, $\kappa = \frac{k_F^2}{9} \frac{\partial^2 E/A}{\partial k_F^2} \sim 14$ MeV [19] at the minimum of the curve,

that should occur at a value of k_F which, when inserted into Eq. (3), provides the experimental density of nuclear matter, namely, 0.17 fm^{-3}.

The three above-mentioned constraints (energy, density, and compressibility) turn out to be fulfilled by choosing

$$\alpha = 0.2, \quad \beta_1 = 0.4, \quad \beta_2 = 4, \tag{9}$$

and

$$U_0 = 2.5 \text{ GeV}, \quad V_0 = 53 \text{ MeV},$$
$$a = 0.465 \text{ fm}, \quad b = 2.10 \text{ fm}. \tag{10}$$

With these values the minimum of the curve yielding E/A versus k_F occurs at $k_F = 1.23$ fm^{-1}, which is obviously different from the value of the pure Fermi gas, namely, $k_F = 1.36$ fm^{-1}.

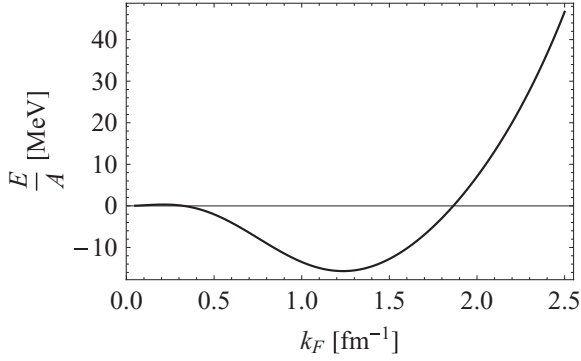FIG. 1. The binding energy (E/A) versus k_F, as given by Eq. (8).

The associated E/A versus k_F is displayed in Fig. 1, which yields

$$\left(\frac{E}{A}\right)_{\min} = -15.68 \text{ MeV},$$
$$(k_F)_{\min} = 1.23 \text{ fm}^{-1}, \quad (\kappa)_{\min} = 13.8 \text{ MeV}, \tag{11}$$

namely, the experimental values.

We also display the momentum distribution $n(k)$ in Fig. 2. Concerning the results of this section, it should be clear that the choice of the parameters given in Eq. (10) is far from unique, and that these values should be viewed as providing a first orientation on a complex problem. Our goal is only to use something representative for the potential in attempting to shed light on the connections between saturation of nuclear matter and electron scattering scaling phenomena. Yet in Sec. V we briefly address the issue of the sensitivity of our results to the values chosen for the parameters, specifically in connection with the pcf and the asymmetry of the scaling function.

III. THE MANY-BODY CONTENT OF $n(k)$ AND THE CSR

Next the following question arises: Which are the Feynman diagrams one has to take into account to obtain the $n(k)$ given by Eq. (2)? This is equivalent to asking what kind of correlations among nucleons are responsible for changing the θ function into our $n(k)$, which we assumed to be the true momentum distribution of our system.
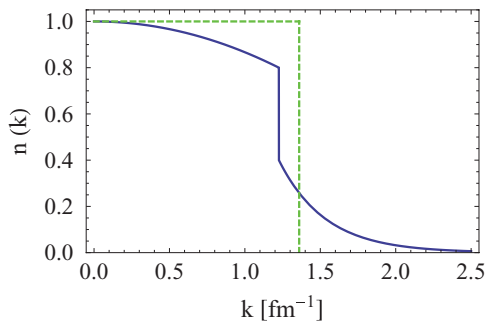

FIG. 2. (Color online) Solid blue line, the momentum distribution $n(k)$ versus k. Also displayed (dashed green line) is the Fermi gas $n(k) = \theta(k_F - k)$ with $k_F = 1.36$ fm^{-1}.
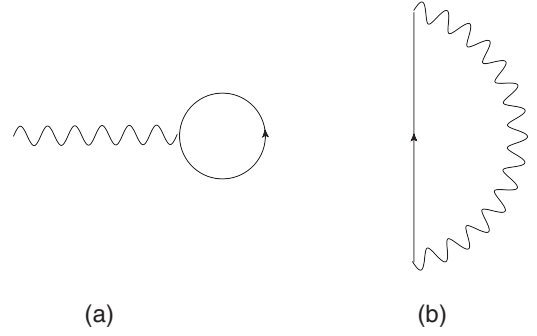

FIG. 3. First-order proper self-energy $\Sigma^\star_{(1)}$. (a),(b) The direct and exchange terms, respectively.

To help in better grasping the relevance of this question it is of importance to realize that if we replace in Eq. (1) $n(k)$ with $\theta(k_F - k)$ and $C(\vec{r}_1 - \vec{r}_2)$ with Eq. (6) we obtain

$$\begin{aligned}
\frac{E}{A} &= \frac{3}{5}\frac{k_F^2}{2m} + n_0\left[\frac{2}{3}\pi a^3 U_0 - \frac{\pi}{4}(b^3 - a^3)V_0\right] \\
&\quad - \frac{1}{\pi}\left(U_0 - \frac{3}{2}V_0\right)\left[\text{Si}(2k_F a) + \frac{\cos(2k_F a) - 3}{2k_F a}\right. \\
&\quad \left. + \frac{\cos(2k_F a) - 1}{2(k_F a)^3} + \frac{\sin(2k_F a)}{(k_F a)^2}\right] \\
&\quad - \frac{3}{2\pi}V_0\left[\text{Si}(2k_F b) + \frac{\cos(2k_F b) - 3}{2k_F b}\right. \\
&\quad \left. + \frac{\cos(2k_F b) - 1}{2(k_F b)^3} + \frac{\sin(2k_F b)}{(k_F b)^2}\right], \tag{12}
\end{aligned}$$

namely, the result provided by HF theory [19], which, as is well known, captures the content of the two first-order perturbative diagrams shown in Fig. 3.

It is instructive to look at the result one gets in HF with the parameters given in Eq. (10) for the double square well potential of Eq. (7). This is displayed in Fig. 4: Here we see that E/A in HF still saturates, although at a far too low density ($k_F = 1.02$ fm^{-1}) and with a far too low energy ($E/A = -1.56$ MeV).

To prove that by summing all perturbative diagrams one would recover the $n(k)$ of Eq. (2) (and hence the E/A of Fig. 1) is clearly an impossibility. In the present study our
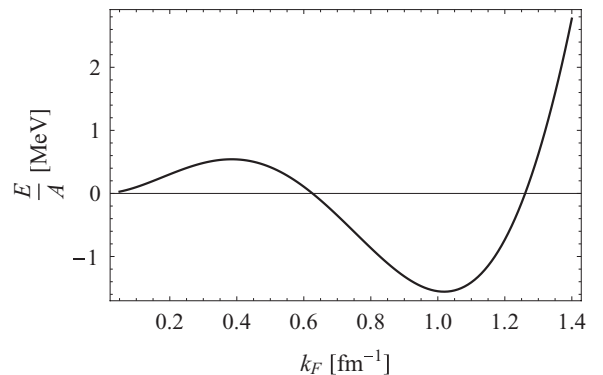

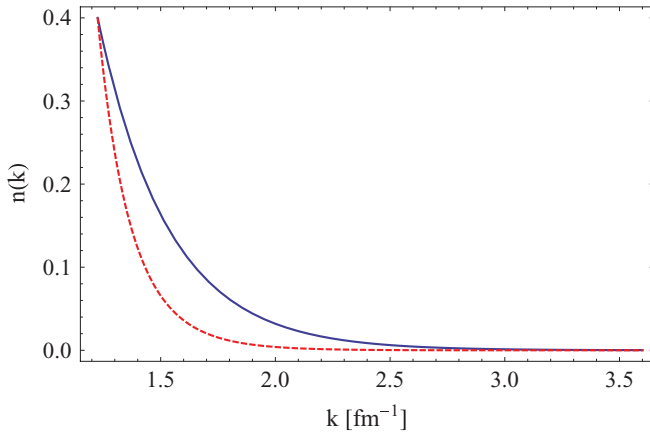FIG. 4. E/A versus k_F in HF theory employing the potential of Eq. (7) with the parameters of Eq. (10).

FIG. 5. (Color online) Solid blue line, the momentum distribution of Eq. (2); dashed red line, Calogero asymptotic behavior Eq. (13), multiplied by a factor 2×10^{-4} (see text for the origin of this factor).

approach is only to explore a simple model while attempting to maintain as high a level of coherence as we can. To achieve the latter we first resort to Calogero's theorem [20], which states that for a homogeneous infinite system asymptotically one should have

$$n(k) \sim \left[2mn_0 \frac{\tilde{v}(k)}{k^2} \right]^2, \tag{13}$$

where, in the present case,

$$
\begin{aligned}
\tilde{v}(k) &= \int d\vec{r} e^{-i\vec{k} \cdot \vec{r}} v(r) \\
&= \frac{4}{3} \pi a^3 \left\{ U_0 \frac{3 j_1(ka)}{ka} - V_0 \left[\frac{b^3}{a^3} \frac{3 j_1(kb)}{kb} - \frac{3 j_1(ka)}{ka} \right] \right\}.
\end{aligned}
\tag{14}
$$

In Fig. 5 we compare our $n(k)$ with the Calogero's theorem predictions: We do so in the range of momenta starting from the Fermi surface ($k = k_F = 1.23$ fm^{-1}) up to $k \sim 3.6$ fm^{-1}, because for larger momenta both distributions become so small that they render the comparison meaningless. In Fig. 5 one sees that the two curves are not too different; hence, our $n(k)$ and $\tilde{v}(r)$, while not exactly the same, nevertheless display an acceptable degree of coherence. It should be stated that in carrying out such a comparison, unfortunately, Calogero's theorem does not quantify the value of q signaling the onset of the asymptotic regime, and hence we have arbitrarily normalized the Calogero's asymptotic momentum distribution in such a way to have it coincide with our $n(k)$ at the Fermi surface.

Concerning the question related to the measurement of $n(k)$, we recall that access to information on this is offered by the CSR, which, in fact, essentially depends "only" upon the momentum distribution at least within the context of the present model. Indeed, from unitarity one has

$$S(q) = Z - n_0^2 V \frac{1}{2} \int d\vec{r} e^{-i\vec{q} \cdot \vec{r}} g^2(r), \tag{15}$$

where $g(r)$ [see Eq. (5)] is directly fixed by the Fourier transform of our $n(k)$.
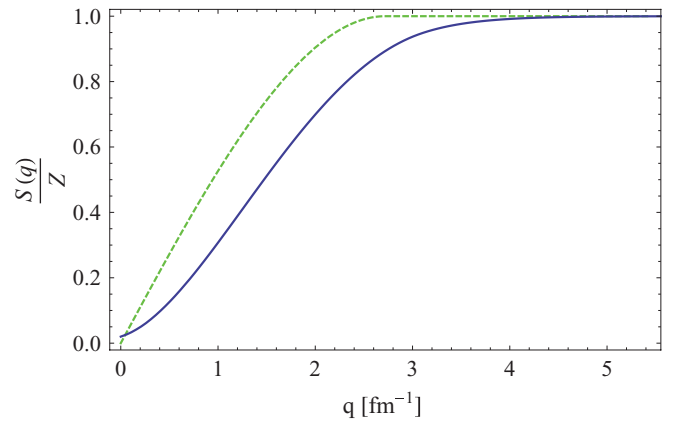

FIG. 6. (Color online) The CSR for a free Fermi gas (dashed green line) and for a correlated one according to our model (solid blue line).

For the sake of completeness, we display in Fig. 6 the CSR predicted by our $n(k)$. Actually, this curve was already shown in Ref. [12]; however, we revisit it once more here to illustrate how the attainment of the asymptotic value (namely, one) is postponed by the nucleon-nucleon correlations, in particular, the repulsive short-range ones, to larger values of q ($\cong 4.6$ fm^{-1}) than for the Fermi gas situation ($\cong 2.46$ fm^{-1}).

To illustrate our second path toward coherence we commence by recalling the alternative model of Ref. [21], which deals with the same issues treated in the present paper, namely, the scaling function and momentum distribution, but with a different philosophy. The study of Ref. [21] is based on the use of PWIA (plane-wave impulse approximation) and has as its starting point the assumption of the factorization of the one-particle exclusive cross section [namely, the cross section for the process $(e, e'N)$] according to the expression

$$\left[\frac{d\sigma}{d\epsilon' d\Omega' dp_N d\Omega_N} \right]^{\text{PWIA}} = K \sigma^{eN}(q, \omega; p, \mathcal{E}, \phi_N) S(p, \mathcal{E}). \tag{16}$$

In the above, K is a kinematical factor, σ^{eN} the eN single-nucleon cross section, and $S(p, \mathcal{E})$ the nucleon spectral function expressed in terms of the so-called missing-energy and missing-momentum variables (for their definition see, for instance, Ref. [22]). We do not dwell here on the procedure leading from Eq. (16) to the scaling function: This topic has been addressed a number of times in the literature. Suffice it to say that the key step is the integration of Eq. (16) over the variables p and $\mathcal{E}$ in a domain which has been analyzed in the past and whose boundaries are set by energy and momentum conservation. The above procedure corresponds to passing from the semi-inclusive $(e, e'N)$ cross section to the inclusive (e, e') cross section. Indeed, one has

$$\frac{d\sigma}{d\epsilon' d\Omega'} = \overline{\sigma}^{eN}(q, \omega; p = |y|, \mathcal{E} = 0) F(q, \omega), \tag{17}$$

where $\overline{\sigma}^{eN}$ is evaluated at the minimum values of $\mathcal{E}$ and p allowed by kinematics and $F(q, \omega)$, referred to as the scaling

function, is easily found to read

$$F(q, \omega) = 2\pi \iint_{\Sigma(q,\omega)} p\, dp\, d\mathcal{E}\, S(p, \mathcal{E}) \tag{18}$$

in PWIA. Now if the integration domain $\Sigma(q, \omega)$ in Eq. (18) extends up to encompass the limiting value $\mathcal{E} \to \infty$, then the scaling function can be linked to the momentum distribution according to [23]

$$n(p) = \int_0^\infty d\mathcal{E}\, S(p, \mathcal{E}). \tag{19}$$

Thus, at variance with our method, which is based on the coherence between the momentum distribution and the scaling function, in the sense of having both of them emerge within the same theory, in Ref. [21] the strategy is to exploit the link between the scaling function and the momentum distribution and hence the possibility of extracting information on $n(k)$ from (e, e') experimental data.

IV. SETTING UP THE SINGLE-NUCLEON PROPAGATOR

Our scheme is based on the central role played by the single-fermion propagator $G(\vec{k}, \omega)$ for nucleons in the nucleus. In fact, as is well known, knowledge of the latter gives access to the E/A according to the expression [24]

$$E = \frac{iV}{2(2\pi)^4} \lim_{\eta \to 0^+} \int d\vec{k} \int_{-\infty}^\infty d\omega\, e^{i\omega\eta} \left(\frac{k^2}{2m} + \omega \right) \mathrm{Tr} G(\vec{k}, \omega) \tag{20}$$

and to the scaling function according to the formula

$$F(q, \omega) = -\frac{q}{m} \frac{V}{\pi} \mathrm{Im} \Pi(q, \omega). \tag{21}$$

This represents the content of linear response theory and, as in Ref. [21], assumes the factorization of the single-nucleon cross section. In Eq. (21) $\Pi(q, \omega)$ is referred to as the polarization propagator or, in coordinate space, as the density-density correlation function. In field-theory language it corresponds to a particular choice of the field arguments in the two-particle propagator and in momentum space reads

$$\Pi(q, \omega) = -\frac{i}{2} \int \frac{d^4k}{(2\pi)^4} G(k + q) G(k). \tag{22}$$

Knowing G ensures control of $\Pi(q, \omega)$ and this, in turn, through Eq. (21), permits the determination of the scaling function $F(q, \omega)$. Also, in a coherent scheme, $G(k)$ should yield the correct momentum distribution [namely, our $n(k)$].

Can such a propagator be derived on the basis of the knowledge of $n(k)$ alone? The answer is yes in the simple approach taken in the present work where an infinite, homogeneous many-body system of nucleons has been assumed. In this framework we propose a kind of mean-field approximation for G which, however, possesses a remarkably coherent structure; whether this remains true in a more sophisticated many-body framework has yet to be proven. Continuing to work within the context of our simple model, as a first step to achieve this goal we rewrite our basic expression in Eq. (1), exploiting the Faltung theorem of Fourier analysis. For this purpose, we start from

$$\begin{aligned}
\frac{E}{A} &= \frac{4V}{A} \int \frac{d\vec{k}}{(2\pi)^3} \frac{k^2}{2m} n(k) + \frac{n_0}{2} \int d\vec{r}\, v(r) \left(1 - \frac{1}{4} g^2(r) \right) \\
&= \frac{4}{n_0} \int \frac{d\vec{k}}{(2\pi)^3} \frac{k^2}{2m} n(k) + \frac{n_0}{2} \left[\int d\vec{r}\, v_D(r) \right. \\
&\quad \left. - \frac{1}{4} \int d\vec{r}\, v_E(r) g^2(r) \right],
\end{aligned} \tag{23}$$

with $g^2(r)$ given by Eq. (4) and the direct and the exchange potential terms by Eq. (8) in coordinate space and introducing the Fourier representations according to

$$\tilde{v}_D(k) = \int d\vec{r}\, e^{-i\vec{k}\cdot\vec{r}} v_D(r) = \frac{4\pi}{3} U_0 a^3 \frac{3 j_1(ka)}{ka} - \frac{\pi}{2} V_0 \left(b^3 \frac{3 j_1(kb)}{kb} - a^3 \frac{3 j_1(ka)}{ka} \right), \tag{24}$$

$$\tilde{v}_E(k) = \int d\vec{r}\, e^{-i\vec{k}\cdot\vec{r}} v_E(r) = \frac{4\pi}{3} \left[a^3 \frac{3 j_1(ka)}{ka} \left(U_0 - \frac{3}{2} V_0 \right) + \frac{3}{2} V_0 b^3 \frac{3 j_1(kb)}{kb} \right] \tag{25}$$

and

$$\int d\vec{r}\, e^{-i\vec{k}\cdot\vec{r}} \left(1 - \frac{1}{4} g^2(r) \right) = (2\pi)^3 \delta(\vec{k}) - \frac{4}{n_0^2} h^2(\alpha, \beta_1, \beta_2) \int \frac{d\vec{p}}{(2\pi)^3} n(p) n(|\vec{k} - \vec{p}|). \tag{26}$$

Then, with the help of Eqs. (24)–(26), we obtain

$$\frac{E}{A} = \frac{4}{n_0} \int \frac{d\vec{k}}{(2\pi)^3} n(k) \left[\frac{k^2}{2m} + \frac{n_0}{2} \tilde{v}_D(0) - \frac{h^2(\alpha, \beta_1, \beta_2)}{2} \int \frac{d\vec{q}}{(2\pi)^3} n(q) \tilde{v}_E(|\vec{k} + \vec{q}|) \right] = \frac{4}{n_0} \int \frac{d\vec{k}}{(2\pi)^3} \epsilon_k^{(h)}, \tag{27}$$

where

$$\epsilon_k^{(h)} = n(k) \left[\frac{k^2}{2m} + \frac{n_0}{2} \tilde{v}_D(0) - \frac{h^2(\alpha, \beta_1, \beta_2)}{2(2\pi)^2} \int_0^\infty dp\, p^2 \tilde{v}_E(p) \int_{-1}^1 dx\, n(|\vec{p} - \vec{k}|) \right] \tag{28}$$

is the single-hole energy displayed in Fig. 7. For comparison, in Fig. 8 the single-particle energy

$$\epsilon_k^{(p)} = \frac{1 - n(k)}{n(k)} \epsilon_k^{(h)} \tag{29}$$

is shown. Note the discontinuity of $\sim$6.5 MeV in both $\epsilon_k^{(h)}$ and $\epsilon_k^{(p)}$ at the Fermi surface, the vanishing at large k of $\epsilon_k^{(h)}$, and the value

$$
\begin{aligned}
\epsilon_0^{(h)} &= \frac{n_0}{2} \tilde{v}_D(0) - \frac{h^2(\alpha, \beta_1, \beta_2)}{(2\pi)^2} \int_0^\infty dp p^2 \tilde{v}_E(p) n(p) = \frac{n_0}{2} \frac{4\pi}{3} a^3 \left[U_0 - \frac{3}{8} V_0 \left(\frac{b^3}{a^3} - 1 \right) \right] \\
&\quad - \frac{h^2(\alpha, \beta_1, \beta_2)}{\pi} \left\{ \left(U_0 - \frac{3}{2} V_0 \right) [\mathrm{Si}(k_F a) - (1 - \alpha) \sin(k_F a) - 3\alpha j_1(k_F a)] \right. \\
&\quad + \frac{3}{2} V_0 [\mathrm{Si}(k_F b) - (1 - \alpha) \sin(k_F b) - 3\alpha j_1(k_F b)] \\
&\quad + \beta_1 \left(U_0 - \frac{3}{2} V_0 \right) \left[k_F a \frac{k_F a \sin(k_F a) - \beta_2 \cos(k_F a)}{(k_F a)^2 + \beta_2^2} + e^{\beta_2} \mathrm{Im} E_1(\beta_2 - ik_F a) \right] \\
&\quad \left. + \beta_1 \frac{3}{2} V_0 \left[k_F b \frac{k_F b \sin(k_F b) - \beta_2 \cos(k_F b)}{(k_F b)^2 + \beta_2^2} + e^{\beta_2} \mathrm{Im} E_1(\beta_2 - ik_F b) \right] \right\} = -77.90 \text{ MeV} \tag{30}
\end{aligned}
$$

of the latter at the origin. The above single-particle energies yield the poles of the fermion propagator which, as a consequence, can then be cast into the form

$$
\begin{aligned}
G(k, \omega) &= \frac{n(k)}{\omega - n(k)\left[\frac{k^2}{2m} + \frac{n_0}{2}\tilde{v}_D(0) - \frac{h^2(\alpha,\beta_1,\beta_2)}{2(2\pi)^2} \int_0^\infty dp p^2 \tilde{v}_E(p) \int_{-1}^1 dx n(|\vec{p} - \vec{k}|) \right] - i\eta} \\
&\quad + \frac{1 - n(k)}{\omega - [1 - n(k)]\left[\frac{k^2}{2m} + \frac{n_0}{2}\tilde{v}_D(0) - \frac{h^2(\alpha,\beta_1,\beta_2)}{2(2\pi)^2} \int_0^\infty dp p^2 \tilde{v}_E(p) \int_{-1}^1 dx n(|\vec{p} - \vec{k}|) \right] + i\eta}. \tag{31}
\end{aligned}
$$

This structure of the propagator tells us that in our model the holes (associated with the poles in the upper energy plane) exist below, but also above, the Fermi surface. Likewise, the particles (associated with the poles in the lower energy plane) exist above, but also below, the Fermi surface. These occurrences clearly reflect the behavior of our momentum distribution. The important point to be stressed, however, is that the propagator in Eq. (31) provides the correct system energy and $n(k)$.

Now, to pave the way to the actual evaluation of Π, it helps to realize that, although the expression of the single-particle energies is far from being simple (in fact, it cannot be expressed analytically), nevertheless its k dependence lends itself to be suitably represented, apart from the factor $n(k)$, by a parabola. This is reminiscent of HF theory. Hence, we use the following quite faithful representation:

$$\epsilon^{(h)}(k) = n(k)(A_{(h)} + B_{(h)} k^2) = n(k)\left(A_{(h)} + \frac{k^2}{2m_{(h)}^\star} \right), \tag{32}$$

with $A_{(h)} = -77.16$ MeV and $B_{(h)} = 41.10$ MeV fm^2, yielding an effective mass $m_{(h)}^\star = 0.50\, m$ for holes and

$$
\begin{aligned}
\epsilon^{(p)}(k) &= [1 - n(k)](A_{(p)} + B_{(p)} k^2) \\
&= [1 - n(k)]\left(A_{(p)} + \frac{k^2}{2m_{(p)}^\star} \right), \tag{33}
\end{aligned}
$$

with $A_{(p)} = -43.09$ MeV and $B_{(p)} = 22.72$ MeV fm^2, yielding an effective mass $m_{(p)}^\star = 0.91\, m$ for particles. It is indeed startling to realize how large the impact of our two-body interaction in Eq. (7) is on the effective hole mass, the generally accepted ratio being actually $m^*/m \simeq 0.83$ [25]. How faithful Eqs. (32) and (33) are in providing the single-particle energies can be garnered from Figs. 7 and 8.
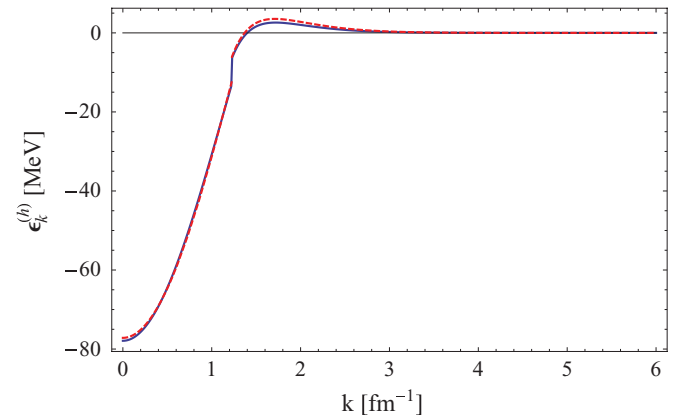

FIG. 7. (Color online) Single-particle energy (hole) of our model shown for $k_F = 1.23$ fm^{-1}, which corresponds to the saturation density of the system. The dashed line represents the fit given by Eq. (32).
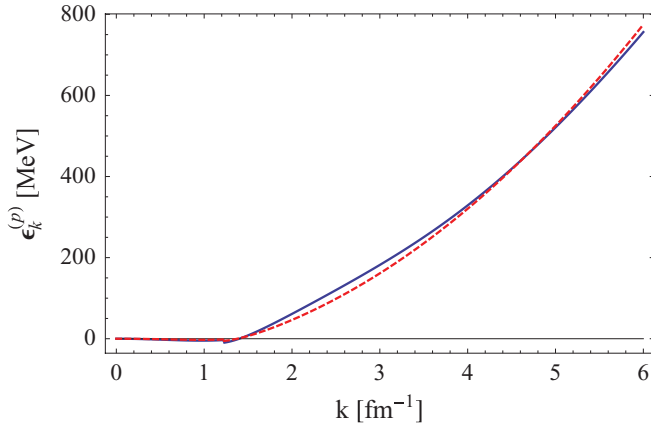
FIG. 8. (Color online) Single-particle energy (particle) of our model shown for $k_F = 1.23$ fm^{-1}, which corresponds to the saturation density of the system. The dashed line represents the fit given by Eq. (33).

Finally, the response function of the system is easily derived,

$$R(q, \omega) = -\frac{V}{\pi} \text{Im}\Pi(q, \omega), \qquad (34)$$

and from the response one immediately obtains the scaling function per proton according to

$$
\begin{aligned}
F(q, \omega) &= \frac{q}{m} \frac{R(q, \omega)}{Z} \\
&= \frac{q}{m} \frac{1}{n_0} \frac{1}{\pi^2} \int_0^\infty dk\, k^2 n(k) \int_{-1}^1 dx [1 - n(|\vec{k} + \vec{q}|)]\delta \\
&\quad \times [\omega - \epsilon^{(p)}(|\vec{k} + \vec{q}|) + \epsilon^{(h)}(k)],
\end{aligned}
\qquad (35)
$$

where the trivial frequency and azimuthal integrations have been performed. The results of our numerical calculations of Eq. (35) are reported in the next section. Following standard practice when discussing scaling we show results for the dimensionless scaling function

$$f(q, \omega) \equiv k_F \times F(q, \omega), \qquad (36)$$

which takes on an especially simple form for the relativistic Fermi gas (see, e.g., Refs. [2,3]).

V. RESULTS

In Figs. 9 and 10 the results for the response $R(q, \omega)$ [Eq. (34)] and scaling function $f(q, \omega)$ [Eq. (36)] are shown versus ω for a range of momentum transfers. The response and the scaling function for the free Fermi gas are also displayed for comparison.

We observe the following.

(i) The response and scaling function obtained using our model, as expected, span a range of energy loss that extends to larger values than that seen for the Fermi gas model, a clear indication of the role of correlations among the nucleons. The widths seen in our model are somewhat larger than those the Fermi gas and the
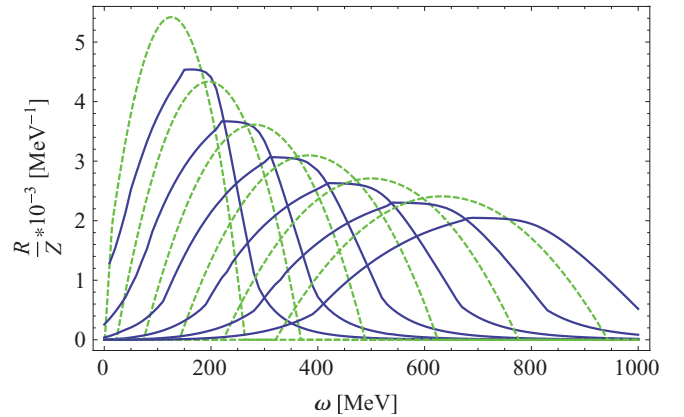

FIG. 9. (Color online) The response function of our model (solid blue line) and the response function of a free Fermi gas (dashed green line) plotted versus ω for $q = 2k_F = 2.46$ fm^{-1} up to $q = 4.5k_F = 5.53$ fm^{-1} in steps of $0.5k_F$. Results for lower values of q peak at lower values of ω.

peak heights are somewhat lower, both in better accord with experimental data.

(ii) The peak positions in our model are shifted to higher energy loss than for the Fermi gas (see also the discussions to follow).

(iii) Unlike for the Fermi gas model, our $R(q, \omega)$ and $f(q, \omega)$ are no longer perfectly symmetric around their maxima. While approximately so, they have tails that extend both to higher and to lower values of ω. However, the degree of asymmetry is not as large as what is observed experimentally.

(iv) Note that while the height of $R(q, \omega)$ decreases with q, the height of $f(q, \omega)$ remains constant.

To investigate the scaling behavior of our results we follow the usual procedures and display f, not versus ω as above, but versus the well-known nonrelativistic scaling variable [26]

$$\psi_{\text{nr}} = \frac{1}{k_F}\left(\frac{m\omega}{q} - \frac{q}{2}\right). \qquad (37)$$
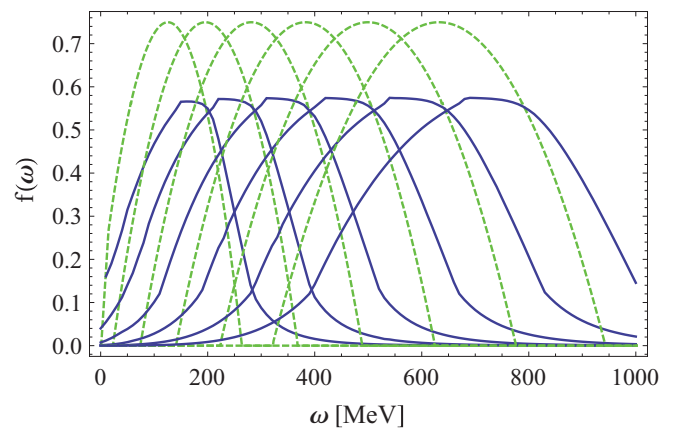

FIG. 10. (Color online) The scaling function of our model (solid blue line) and the scaling function of a free Fermi gas (dashed green line) plotted versus ω for the same values of q used in Fig. 9.
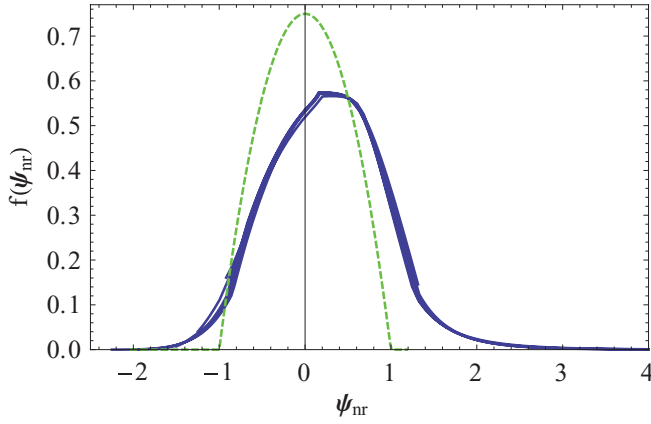
FIG. 11. (Color online) The scaling function of our model (blue line) displayed versus the nonrelativistic variable ψ_{nr}. The momentum transfer range is the same as in the previous two figures. For reference the Fermi gas result is shown as a dashed green curve; clearly, by construction, it scales perfectly.

Now we indeed see in Fig. 11 that the scaling functions for different values of q tend to group together very closely when displayed versus ψ_{nr}; that is, they scale. Noting that the coalescence in our model occurs at a peak value other than $\psi_{nr} = 0$, it is interesting to investigate whether a simple modification of the scaling variable different from the one of Eq. (37) can be devised to shift the peak position to zero. One can always do this by employing the variable

$$\psi'_{nr} \equiv \frac{1}{k_F}\left(\frac{m\omega'}{q} - \frac{q}{2}\right), \tag{38}$$

where $\omega' = \omega - E_{shift}(q)$, and where $E_{shift}(q)$ is a q-dependent energy shift. If one uses the simple parametrization

$$E_{shift}(q) = E_0 + E_1(q/k_F), \tag{39}$$

with $E_0 = -17.4$ MeV and $E_1 = 15.9$ MeV (see Fig. 13), then almost perfect scaling centered about $\psi'_{nr} = 0$ is attained, as seen in Fig. 12. It appears that the impact of the NN interactions that have been incorporated in the present model is felt via a q-dependent shift in the definition of this new scaling variable, although a direct connection to the underlying dynamics is not obvious. As is clear from Fig. 13 similar shifting is seen using relativistic mean-field theory. One, of course, should not expect these to be identical, because the present model is nonrelativistic while the RMF results are obtained using a relativistic model. In either case, while the shift is qualitatively what is observed experimentally, it is probably somewhat too strong in both cases [27,28].

In Fig. 14 we show the same results as in Fig. 12, but now on a semilog scale. The asymmetry, while small, is clearly apparent. More strength is shifted to higher values of ψ'_{nr} and, whereas the Fermi gas cuts off abruptly and is only nonzero within the Fermi cone, the present model produces strength extending to very large and small values of ψ'_{nr}, in accord with experiment. It is worth remarking that if the high momentum tail in the momentum distribution in Eq. (2) is set to zero (i.e., β_1 is set to zero) then these tails extending to large $|\psi'_{nr}|$ essentially disappear. While setting β_1 to zero is not
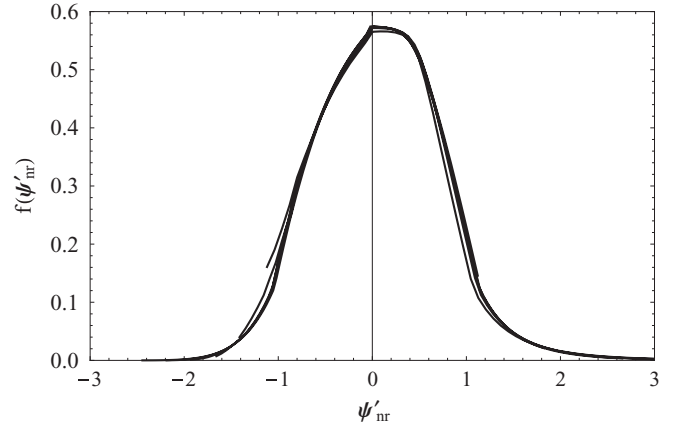

FIG. 12. The scaling function of our model displayed versus the scaling variable of Eq. (38) for the same values of q used in Fig. 11.

simply setting the part of the momentum distribution arising from short-range correlations to zero, because the long-range correlations also move some strength from below the Fermi surface to somewhat above it, it is very suggestive that in the present model the origin of the tails in the scaling function are principally attributable to the short-range physics, as is often assumed to be the case. Interestingly, the position of the peak is largely unaffected by "turning off" the high-k part of the momentum distribution, suggesting that the peak position is not strongly correlated with the short-range physics, but rather with the long-range physics.

As previously anticipated, aiming at a deeper understanding of the role of the tail of $n(k)$ of our results, and thus exploring the sensitivity to variations of the parameters, we have repeated the entire calculation using a stronger high-momentum tail. The latter is ruled by the parameters β_1 and β_2: We have found a strong sensitivity to β_2, which controls the extension of the tail. Indeed, with β_2 small enough, that is, with a long tail, the pcf becomes negative at short distances and thus physically unacceptable. We have therefore limited ourselves to varying only β_1. In particular, we have performed the calculations with $\beta_1 = 0.65$ (to be compared with the previous value
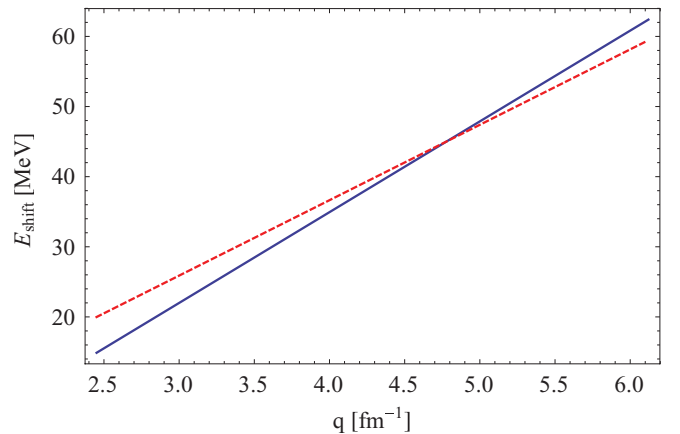

FIG. 13. (Color online) The q-dependent energy shift in Eq. (39) (solid blue curve) together with the energy shift obtained in RMF studies of ^{12}C (dashed red curve).
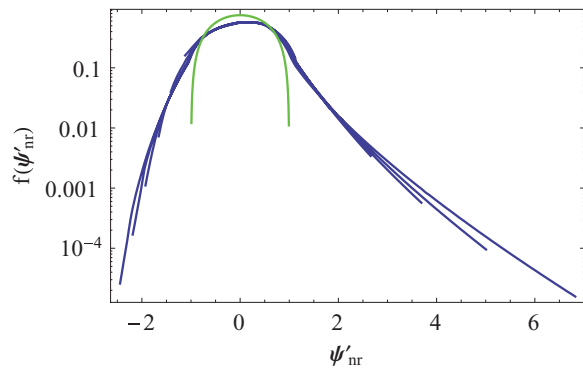
FIG. 14. (Color online) As for Fig. 12, but now on a semilog scale.

FIG. 16. The scaling function versus q for $[\psi'_{nr}]_0 = -0.6, -0.4$, and -0.2, that is, in the scaling region.

$\beta_1 = 0.4$), namely, with a tail for the momentum distribution that is somewhat stronger. Also in this case we are able to reproduce the density, binding energy, and compressibility, and also in this case we find scaling. However, interestingly, the scaling function occurring in this case is found to be more asymmetric than the previous one, as shown in Fig. 15. This raises important issues on the origin of the experimental asymmetry of the scaling function.

In concluding this section we address the problem of how the scaling regime is approached. We do so using the scaling variable $[\psi'_{nr}]_0$, where, to make this closer to what has been used in analyses of experimental data [1] a constant energy shift $E_{shift} = 30$ MeV has been chosen in using Eq. (38); this is indicated by the subscript "0". We display f as a function of q for three values of the scaling variable in the scaling region, that is, to the left of the QE peak. The curves are shown normalized at $q = 2k_F$, namely, the ratio

$$\rho(q) \equiv f(q, [\psi'_{nr}]_0)/f(2k_F, [\psi'_{nr}]_0) \qquad (40)$$

is displayed. From Fig. 16 it clearly appears that the scaling regime is approached from above, an occurrence that is qualitatively in accord with experimental findings.
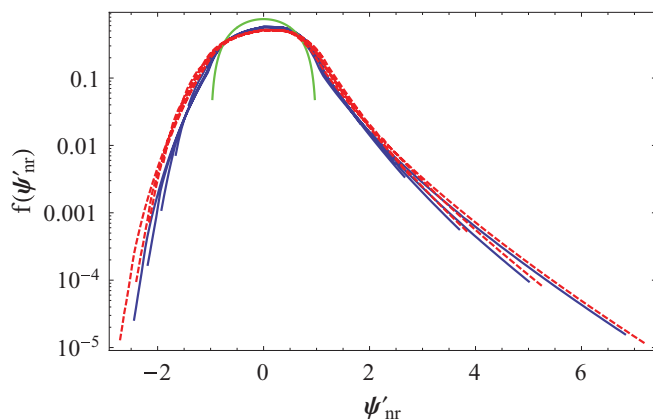

FIG. 15. (Color online) As for Fig. 14, but now adding (dashed red curves) the results obtained with a different set of parameters: $a = 0.464$ fm, $b = 1.917$ fm, $U_0 = 2.9$ GeV, $V_0 = 48$ MeV, $\alpha = 0.2$, $\beta_1 = 0.65$, $\beta_2 = 4$.
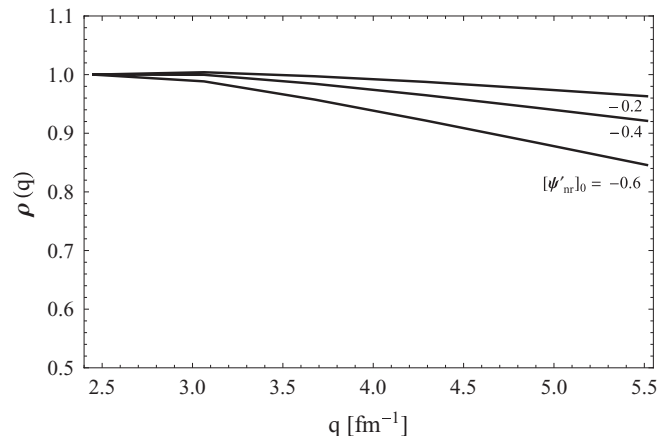
VI. CONCLUSIONS

In the present study we have developed a model centered around an assumed form for the momentum distribution of nucleons in nuclei. The momentum distribution has been chosen to reflect current understanding of how dynamical effects underlying the nuclear many-body problem lead to a form for $n(k)$ with low- and high-k components coming from both long- and short-range NN interactions. For the present, we have restricted the scope of the study to infinite, homogeneous nuclear matter, have employed only point nucleons, have assumed a strictly nonrelativistic model (although in future work we hope to extend the scope to relativistic modeling), and have restricted our attention to the longitudinal electromagnetic response.

Working with this as a basis we have developed the formalism in two different directions, maintaining as much consistency as possible. First, we have devised a single-particle Green's function that leads to the known saturation properties of nuclear matter and to realistic particle and hole single-particle energy spectra. Second, we have taken the same Green's function to obtain the density-density polarization propagator and, through its imaginary part, have obtained the longitudinal electron scattering response function $R(q, \omega)$ and the scaling function $f(q, \omega)$. For the latter we have explored several aspects of scaling and of scaling violations.

We find that scaling is quite well respected, despite the strength of the NN interactions implicit in the problem. There are seen to be some scaling violations, for instance, those observed as shifts of the quasielastic peak positions as functions of q; indeed, these are also seen in relativistic mean-field theory. The shape of the scaling function is observed to be more spread out than is the Fermi gas scaling function and the former yields a somewhat lower peak height than the latter, both in rough accord with experiment. Where it is large the scaling function in our model is somewhat asymmetric; however, it is not enough so to agree with experiment. When the tails of the scaling function are examined in detail the asymmetry is more apparent and, indeed, the strength at both very large and very small values of the scaling variable is significant, in accord with experiment. If the high-k contributions to

the momentum distribution are "turned off" then these tails disappear, suggesting that their origin lies in the part of the momentum distribution arising from short-range correlations. The position of the peak, however, appears to be attributable to long-range physics.

We are, of course, aware that our modeling of the propagator is rather simplistic: Its poles do not lie close to the real axis, but actually move in the complex energy plane. This occurs, in particular, in the presence of a strong short-range NN force, as shown, for instance, by the work of Sartor and Mahaux [29]. We are currently working in the direction of extending our approach to single-particle states with finite lifetimes and accounting for the modification of the Green's function owing to correlations.

To clarify further the role of the strong short-range repulsion (srr), namely, where it is active, we refer again to past work on the hard-sphere Fermi gas [29], that is, a system of fermions interacting only via a strong srr. This study computes the momentum distribution $n(k)$ accounting for the so-called correlation (or rearrangement) second-order diagrams. It is plainly apparent from it that the srr modifies $n(k)$ with respect to the pure Fermi gas not only in the high-momentum tail but also in the range $0 < k < k_F$, the only interval where the Pauli correlations are active; these alone would yield, of course, the well-known step-function distribution.

In summary, the present study has demonstrated that a high level of consistency can be maintained in simultaneously representing both the saturation properties of nuclear matter and the scaling properties of the longitudinal electron scattering response.

Before concluding, we would like to stress once more that the main purpose of the paper has been to tie the ground-state properties, as embodied by the Green's function, to the particle-hole propagator, the EM response, and scaling. This could be achieved, all strictly numerically, with the most sophisticated $n(k)$ existing in the literature; however, our approach has been to employ a "reasonable" parametrization to keep the formalism analytically tractable as long as possible.

[1] D. B. Day, J. S. McCarthy, T. W. Donnelly, and I. Sick, Annu. Rev. Nucl. Part. Sci. **40**, 357 (1990).

[2] T. W. Donnelly and I. Sick, Phys. Rev. Lett. **82**, 3212 (1999).

[3] T. W. Donnelly and I. Sick, Phys. Rev. C **60**, 065502 (1999).

[4] A. N. Antonov, M. V. Ivanov, M. B. Barbaro, J. A. Caballero, and E. M. de Guerra, Phys. Rev. C **79**, 044602 (2009).

[5] J. A. Caballero, J. E. Amaro, M. B. Barbaro, T. W. Donnelly, and J. M. Udias, Phys. Lett. B **653**, 366 (2007).

[6] J. E. Amaro, M. B. Barbaro, J. A. Caballero, T. W. Donnelly, and A. Molinari, Phys. Rep. **368**, 317 (2002).

[7] A. De Pace, M. Nardi, W. M. Alberico, T. W. Donnelly, and A. Molinari, Nucl. Phys. A **726**, 303 (2003).

[8] A. De Pace, M. Nardi, W. M. Alberico, T. W. Donnelly, and A. Molinari, Nucl. Phys. A **741**, 249 (2004).

[9] J. E. Amaro, M. B. Barbaro, J. A. Caballero, T. W. Donnelly, C. Maieron, and J. M. Udias, Phys. Rev. C **81**, 014606 (2010).

[10] J. E. Amaro, C. Maieron, M. B. Barbaro, J. A. Caballero, and T. W. Donnelly, Phys. Rev. C **82**, 044601 (2010).

[11] G. Parisi, *Field Theory, Disorder and Simulations* (World Scientific, Singapore, 1992), p. 66.

[12] M. B. Barbaro, D. Berardo, R. Cenni, T. W. Donnelly, and A. Molinari, Phys. Rev. C **80**, 064320 (2009).

[13] K. Gottfried, Ann. Phys. **21**, 29 (1963).

[14] A. N. Antonov, M. V. Ivanov, J. A. Caballero, M. B. Barbaro, J. M. Udias, E. Moya de Guerra, and T. W. Donnelly, Phys. Rev. C **83**, 045504 (2011).

[15] H. Muther, G. Knehr, and A. Polls, Phys. Rev. C **52**, 2955 (1995).

[16] H. Muther, A. Polls, and W. H. Dickhoff, Phys. Rev. C **51**, 3040 (1995).

[17] J. W. Van Orden, W. Truex, and M. K. Banerjee, Phys. Rev. C **21**, 2628 (1980).

[18] A. N. Antonov, M. K. Gaidarov, M. V. Ivanov, D. N. Kadrev, G. Z. Krumova, P. E. Hodgson, and H. V. von Geramb, Phys. Rev. C **65**, 024306 (2002).

[19] W. M. Alberico, R. Cenni, and A. Molinari, La Rivista del Nuovo Cimento **1**, N.4 (1978).

[20] R. D. Amado, Phys. Rev. C **14**, 1264 (1976).

[21] J. A. Caballero, M. B. Barbaro, A. N. Antonov, M. V. Ivanov, and T. W. Donnelly, Phys. Rev. C **81**, 055502 (2010).

[22] R. Cenni, T. W. Donnelly, and A. Molinari, Phys. Rev. C **56**, 276 (1997).

[23] Note that a different normalization for the momentum distribution is adopted in Refs. [21,22].

[24] A. L. Fetter and J. D. Walecka, *Quantum Theory of Many-Particle Systems* (McGraw-Hill, San Francisco, 1971), p. 69.

[25] C. H. Johnson, D. J. Horen, and C. Mahaux, Phys. Rev. C **36**, 2252 (1987).

[26] W. M. Alberico, A. Molinari, T. W. Donnelly, E. L. Kronenberg, and J. W. Van Orden, Phys. Rev. C **38**, 1801 (1988).

[27] J. A. Caballero, Phys. Rev. C **74**, 015502 (2006).

[28] J. E. Amaro, M. B. Barbaro, J. A. Caballero, T. W. Donnelly, and J. M. Udias, Phys. Rev. C **75**, 034613 (2007).

[29] R. Sartor and C. Mahaux, Phys. Rev. C **21**, 1546 (1980).